

A comparative study of three domain-integral evaluation techniques in the boundary-domain integral equation method for transient thermoelastic crack analysis in FGMs

A.V. Ekhlakov^{1,2}, O.M. Khay^{1,3}, Ch. Zhang¹, X.W. Gao⁴,
J. Sladek⁵ and V. Sladek⁵

Abstract: A boundary-domain integral equation method is applied to the transient thermoelastic crack analysis in functionally graded materials. Fundamental solutions for homogeneous, isotropic and linear elastic materials are used to derive the boundary-domain integral equations. The radial integration method, the Cartesian transformation method and the cell-integration method are applied for the evaluation of the arising domain-integrals. Numerical results for dynamic stress intensity factors obtained by the three approaches are presented, compared and discussed to show the accuracy and the efficiency of the domain-integral evaluation techniques.

Keywords: Radial integration method, Cartesian transformation method, cell-integration method, dynamic stress intensity factors, functionally graded materials.

1 Introduction

Functionally graded materials (FGMs) represent a new class of composite materials formed by continuously changing composition of constituents in space. Compared to the conventional composite materials, FGMs possess many superior thermal and mechanical properties as well as corrosion-resistant and wear-resistant properties [Suresh and Mortensen (1998)]. Investigation of the fracture and fatigue properties

¹ Department of Civil Engineering, University of Siegen, D-57068 Siegen, Germany.

² Faculty of Architecture and Civil Engineering, University of Applied Sciences, Kurt-Schumacher-Ring 18, D-65197 Wiesbaden, Germany.

³ Pidstryhach Institute for Applied Problems of Mechanics and Mathematics NASU, 3b Naukova Str., 79060 Lviv, Ukraine.

⁴ Faculty of Vehicle Engineering and Mechanics, Dalian University of Technology, 116024 Dalian, PR China.

⁵ Institute of Construction and Architecture, Slovak Academy of Sciences, 84503 Bratislava, Slovakia.

of FGMs under extreme mechanical and thermal loadings is important to their thermal and mechanical integrity, reliability and durability in engineering applications. Thermoelastic fracture analysis may provide a fundamental understanding of and a deep insight into the failure mechanisms of FGMs that may aid in the design, optimisation and applications of FGMs. Due to the high mathematical complexity of the governing equations of transient linear coupled thermoelasticity for FGMs, which are given by the coupled partial differential equations with variable coefficients, advanced numerical methods have to be developed and applied. In principle, the finite element method (FEM) [Keramidas and Ting (1976); Eischen (1987); Anlas; Santare and Lambros (2000); Cannarozzi and Ubertini (2001)], the boundary element method (BEM) [Aliabadi (2002); Balaš; Sládek and Sládek (1989)] and the meshless Petrov-Galerkin method [Sladek; Sladek and Zhang (2005); Sladek; Sladek; Zhang and Tan (2006); Sladek; Sladek; Solek and Atluri (2008a, 2008b); Sladek; Sladek; Solek; Tan and Zhang (2009)] can be applied to the thermoelastic fracture analysis in FGMs. The BEM has been developed and successfully used in homogenous, isotropic and linear elastic solids [Hosseini-Tehrani; Hosseini-Godarzi and Tavangar (2005); Gao; Zhang; Sladek and Sladek (2008)]. Dong and Atluri (2013a, 2013b) have proposed SGBEM-FEM alternating/coupling methods based on weakly-singular Symmetric Galerkin BEM (SGBEM) [Dong and Atluri (2012)]. These methods can be applied to fracture and fatigue analysis curved, branching and intersecting cracks in complex structures. Applications of BEM to continuously non-homogeneous, isotropic and linear elastic solids are very restricted since the required fundamental solutions for the general FGMs are either not available or mathematically extremely complicated. To circumvent this difficulty, a boundary-domain integral equation method (BDIEM) for two-dimensional (2-D) transient linear coupled thermoelastic crack analysis in finite, continuously non-homogeneous, isotropic and linear elastic FGMs subjected to a thermal shock is presented in this paper. The Laplace-transform technique is applied to eliminate the time-dependence in the governing equations. To derive boundary-domain integral equations (BDIEs) the fundamental solutions for homogeneous, isotropic and linear elastic solids are applied. In this case, the BDIEs contain domain integrals, which vanish when the material under investigation is homogeneous. It should be remarked that the BDIE's have been formulated for the primary fields (displacements and temperature) to simplify the analysis. Therefore, the presented BDIEM cannot be directly used in complex structural geometries. From the mathematical point of view there are no limitations to derive the BDIEs for the secondary fields (tractions and thermal flux), for which it is not too difficult to use the proposed method. For fracture analysis curved, branching or intersecting cracks in complex structures can be applied for example the SGBEM-FEM alternated method [Dong and Atluri (2013a, 2013b)]. Since an analytical evaluation of the occurring domain

integrals cannot be carried out in general cases, numerical techniques are required. To this end, the direct technique, the cell-integration method (CIM), can be used, in which the interior of the domain has to be discretized into internal cells. By using this technique, Ekhlakov; Khay; Zhang; Sladek and Sladek (2010, 2012a) have presented the boundary-domain element method for thermoelastic crack analysis. But in the CIM, an important advantage of the BEM is lost due to the domain discretization. Several numerical methods for computing domain integrals have been proposed in the literature over the past years. The most extensively employed methods are the dual reciprocity method (DRM) [Nardini and Brebbia (1983)], multiple reciprocity method [Nowak and Brebbia (1989)] and the fast multipole method [Greengard and Rokhlin (1987)]. A powerful robust transformation technique, the so-called radial integration method (RIM), has been proposed by Gao (2002a, 2002b). It can be applied to any complicated domain integrals including singular ones. The RIM combined with the BEM based on the BDIes has been successfully applied to fracture analysis in FGMs [Gao; Zhang; Sladek and Sladek (2008); Ekhlakov; Khay; Zhang; Sladek; Sladek and Gao (2012b)]. Hematiyan (2007, 2008) has developed the Cartesian transformation method (CTM) to treat domain integrals without any internal cells in the domain of the problem. In the CTM, a domain integral is transformed into a boundary integral and a one-dimensional integral in the Cartesian coordinate system.

This paper is focused on a comparative study of three domain-integral evaluation techniques: the RIM, the CTM and the CIM. A spatial collocation-based BDIEM is developed in the Laplace-transformed domain. To obtain the time-dependent solutions, the Laplace-inversion algorithm by Stehfest (1970) is applied. Numerical examples for computing dynamic stress intensity factors (SIFs) are presented and discussed to compare the accuracy and the efficiency of the three domain-integral evaluation techniques.

2 Problem formulation and boundary-domain integral equations

Let us consider a two-dimensional (2-D), continuously non-homogeneous, isotropic and linear thermoelastic FGM. In the absence of body forces and heat sources, the cracked FGM satisfies the governing equations of transient linear coupled thermoelasticity [Balaš; Sládek and Sládek (1989)]

$$\begin{aligned} \sigma_{ij,j}(\mathbf{x},t) &= \rho(\mathbf{x})\ddot{u}_i(\mathbf{x},t), \\ [k(\mathbf{x})\theta_{,i}(\mathbf{x},t)]_{,i} - \rho(\mathbf{x})c(\mathbf{x})\dot{\theta}(\mathbf{x},t) - k(\mathbf{x})\eta(\mathbf{x})\dot{u}_{k,k}(\mathbf{x},t) &= 0, \end{aligned} \tag{1}$$

the Duhamel-Neumann constitutive equations

$$\sigma_{ij}(\mathbf{x},t) = c_{ijkl}(\mathbf{x})u_{k,l}(\mathbf{x},t) - \gamma(\mathbf{x})\theta(\mathbf{x},t)\delta_{ij}, \tag{2}$$

the initial and boundary conditions

$$\begin{aligned}
 u_i(\mathbf{x},t)|_{t=0} &= \dot{u}_i(\mathbf{x},t)|_{t=0} = 0, & \theta(\mathbf{x},t)|_{t=0} &= 0, \\
 u_i(\mathbf{x},t) &= \widehat{u}_i(\mathbf{x},t), & \mathbf{x} \in \Gamma_u, & \theta(\mathbf{x},t) = \widehat{\theta}(\mathbf{x},t), & \mathbf{x} \in \Gamma_\theta, \\
 t_i(\mathbf{x},t) &= \widehat{t}_i(\mathbf{x},t), & \mathbf{x} \in \Gamma_t, & q(\mathbf{x},t) = \widehat{q}(\mathbf{x},t), & \mathbf{x} \in \Gamma_q, \\
 t_i(\mathbf{x},t) &= 0, & \mathbf{x} \in \Gamma_c & q(\mathbf{x},t) = 0, & \mathbf{x} \in \Gamma_c.
 \end{aligned} \tag{3}$$

In Eqs. (1)-(3), σ_{ij} , u_i and $t_i = \sigma_{ij}n_j$ represent the stress, the displacement and the traction components, θ and $q = -k\theta_{,j}n_j$ are the temperature and the heat flux, \mathbf{x} is the position vector, t is the time variable, n_j are the components of the outward unit normal vector, δ_{ij} denotes the Kronecker symbol, $\gamma(\mathbf{x})$ is the stress-temperature modulus, Γ_u and Γ_t are the parts of the external boundary $\Gamma = \Gamma_u \cup \Gamma_t$, in which the displacements \widehat{u}_i and the tractions \widehat{t}_i are prescribed, Γ_θ and Γ_q are the parts of the external boundary $\Gamma = \Gamma_\theta \cup \Gamma_q$ with the specified temperature $\widehat{\theta}$ and the heat flux \widehat{q} , $\Gamma_c = \Gamma_c^+ \cup \Gamma_c^-$ represents the upper and the lower crack-faces Γ_c^+ and Γ_c^- . The material parameters of the FGM, namely the mass density $\rho(\mathbf{x})$, Young's modulus $E(\mathbf{x})$, thermal conductivity $k(\mathbf{x})$, specific heat $c(\mathbf{x})$ and linear thermal expansion coefficient $\alpha(\mathbf{x})$, are assumed to depend continuously on the Cartesian coordinates, while the Poisson's ratio ν is a constant. In this case, the fourth order elasticity tensor can be written as

$$c_{ijkl}(\mathbf{x}) = \mu(\mathbf{x}) \left[\frac{2\nu}{1-2\nu} \delta_{ij}\delta_{kl} + \delta_{ki}\delta_{lj} + \delta_{kj}\delta_{li} \right] \tag{4}$$

with $\mu(\mathbf{x}) = \frac{E(\mathbf{x})}{2(1+\nu)}$,

where $\mu(\mathbf{x})$ is the shear modulus. Unless otherwise stated, a comma after a quantity represents spatial derivatives, superscript dots indicate time derivatives, the conventional summation rule over double indices is implied, and Latin indices take the values of 1 and 2. Substituting Eqs. (2) and (4) into Eqs. (1) and then applying the Laplace-transform yield

$$\begin{aligned}
 c_{ijkl}\bar{u}_{k,lj} - \gamma\bar{\theta}_{,i} - \rho p^2\bar{u}_i + [c_{ijkl,j}\bar{u}_{k,l} - \gamma_{,i}\bar{\theta}] &= 0, \\
 \bar{\theta}_{,ii} - \frac{p}{\kappa}\bar{\theta} - \eta p\bar{u}_{k,k} + \frac{k_{,i}}{\kappa}\bar{\theta}_{,i} &= 0,
 \end{aligned} \tag{5}$$

where the superimposed bar denotes the Laplace-transformed quantity, p is the Laplace-transform parameter, and $\kappa(\mathbf{x})$ is the thermal conductivity.

The integral representations of the displacements and the temperature at an arbitrary point of the domain are derived from the Betti's reciprocal theorem in conjunction with the fundamental solutions of the Laplace-transformed linear coupled thermoelasticity for homogeneous solids. By moving the observation point to the

boundary $\mathbf{x} \in \Gamma$ or keeping it in the domain $\mathbf{x} \in \Omega$ the following BDIEs for the mechanical and thermal fields are obtained as

$$\begin{aligned} \bar{u}_j(\mathbf{x}, p) &= - \int_{\Gamma} \left[\bar{T}_{ij}(\mathbf{x}, \mathbf{y}, p) \bar{u}_i(\mathbf{y}, p) - \frac{1}{\bar{\gamma}(\mathbf{y})} \bar{U}_{ij}(\mathbf{x}, \mathbf{y}, p) \bar{t}_i(\mathbf{y}, p) \right] d\Gamma_y \\ &\quad + \kappa_0 \int_{\Gamma} \left[\bar{Z}_j(\mathbf{x}, \mathbf{y}, p) \bar{\theta}(\mathbf{y}, p) - \frac{1}{\bar{\eta}(\mathbf{y})} \bar{U}_j(\mathbf{x}, \mathbf{y}, p) \bar{q}(\mathbf{y}, p) \right] d\Gamma_y + \bar{F}_j^{(u)}(\mathbf{x}, p), \\ \bar{\theta}(\mathbf{x}, p) &= \frac{\kappa_0 \eta_0 p}{\gamma_0} \int_{\Gamma} \left[\bar{T}_i(\mathbf{x}, \mathbf{y}, p) \bar{u}_i(\mathbf{y}, p) - \frac{1}{\bar{\gamma}(\mathbf{y})} \bar{U}_i(\mathbf{x}, \mathbf{y}, p) \bar{t}_i(\mathbf{y}, p) \right] d\Gamma_y \\ &\quad - \kappa_0 \int_{\Gamma} \left[\bar{F}(\mathbf{x}, \mathbf{y}, p) \bar{\theta}(\mathbf{y}, p) - \frac{1}{\bar{\eta}} \bar{T}(\mathbf{x}, \mathbf{y}, p) \bar{q}(\mathbf{y}, p) \right] d\Gamma_y + \bar{F}^{(\theta)}(\mathbf{x}, p). \end{aligned} \tag{6}$$

The functions $\bar{F}_j^{(u)}$ and $\bar{F}^{(\theta)}$ are defined as

$$\begin{aligned} \bar{F}_j^{(u)}(\mathbf{x}, p) &= -p^2 \rho_0 \int_{\Omega} \left(\frac{\bar{\rho}(\mathbf{y})}{\bar{\gamma}(\mathbf{y})} - 1 \right) \bar{U}_{ij}(\mathbf{x}, \mathbf{y}, p) \bar{u}_i(\mathbf{y}, p) d\Omega_y + \mu_0 \int_{\Omega} \left[\frac{c_{ikik}^0}{\bar{\alpha}(\mathbf{y})} \frac{\bar{\gamma}_k(\mathbf{y})}{\bar{\gamma}(\mathbf{y})} \bar{U}_{ij}(\mathbf{x}, \mathbf{y}, p) \right. \\ &\quad \left. - \left(\frac{1}{\bar{\alpha}(\mathbf{y})} - 1 \right) \left(\frac{1}{1-2\nu} \delta_{li} \delta_{km} + \delta_{kl} \delta_{im} \right) \bar{U}_{l,j,m}(\mathbf{x}, \mathbf{y}, p) \right] \bar{u}_{i,k}(\mathbf{y}, p) d\Omega_y \\ &\quad + \int_{\Omega} \left[p \left(\frac{1}{\bar{\eta}(\mathbf{y}) \bar{\kappa}(\mathbf{y})} - 1 \right) \bar{U}_j(\mathbf{x}, \mathbf{y}, p) - \gamma_0 \frac{\bar{\gamma}_j(\mathbf{y})}{\bar{\gamma}(\mathbf{y})} \bar{U}_{kk}(\mathbf{x}, \mathbf{y}, p) \right] \bar{\theta}(\mathbf{y}, p) d\Omega_y \\ &\quad + \kappa_0 \int_{\Omega} \left[\left(\frac{1}{\bar{\eta}(\mathbf{y})} - 1 \right) \bar{U}_{j,i}(\mathbf{x}, \mathbf{y}, p) - \frac{1}{\eta_0} \frac{1}{\bar{\eta}(\mathbf{y})} \frac{\bar{\gamma}_i(\mathbf{y})}{\bar{\gamma}(\mathbf{y})} \bar{U}_j(\mathbf{x}, \mathbf{y}, p) \right] \bar{\theta}_{,i}(\mathbf{y}, p) d\Omega_y, \end{aligned} \tag{7}$$

$$\begin{aligned} \bar{F}^{(\theta)}(\mathbf{x}, p) &= \frac{\kappa_0 \eta_0 p}{\gamma_0} \left\{ p^2 \rho_0 \int_{\Omega} \left(\frac{\bar{\rho}(\mathbf{y})}{\bar{\gamma}(\mathbf{y})} - 1 \right) \bar{U}_i(\mathbf{x}, \mathbf{y}, p) \bar{u}_i(\mathbf{y}, p) d\Omega_y - \mu_0 \int_{\Omega} \left[\frac{c_{ikik}^0}{\bar{\alpha}(\mathbf{y})} \frac{\bar{\gamma}_k(\mathbf{y})}{\bar{\gamma}(\mathbf{y})} \right. \right. \\ &\quad \left. \left. \times \bar{U}_i(\mathbf{x}, \mathbf{y}, p) - \left(\frac{1}{\bar{\alpha}(\mathbf{y})} - 1 \right) \left(\frac{1}{1-2\nu} \delta_{li} \delta_{km} + \delta_{kl} \delta_{im} \right) \bar{U}_{l,m}(\mathbf{x}, \mathbf{y}, p) \right] \bar{u}_{i,k}(\mathbf{y}, p) d\Omega_y \right\} \\ &\quad - p \int_{\Omega} \left[\left(\frac{1}{\bar{\eta}(\mathbf{y}) \bar{\kappa}(\mathbf{y})} - 1 \right) \bar{T}(\mathbf{x}, \mathbf{y}, p) - \kappa_0 \eta_0 \frac{\bar{\gamma}_j(\mathbf{y})}{\bar{\gamma}(\mathbf{y})} \bar{U}_j(\mathbf{x}, \mathbf{y}, p) \right] \bar{\theta}(\mathbf{y}, p) d\Omega_y \\ &\quad - \kappa_0 \int_{\Omega} \left[\left(\frac{1}{\bar{\eta}(\mathbf{y})} - 1 \right) \bar{T}_{,i}(\mathbf{x}, \mathbf{y}, p) - \frac{1}{\eta_0} \frac{1}{\bar{\eta}(\mathbf{y})} \frac{\bar{\gamma}_i(\mathbf{y})}{\bar{\gamma}(\mathbf{y})} \bar{T}(\mathbf{x}, \mathbf{y}, p) \right] \bar{\theta}_{,i}(\mathbf{y}, p) d\Omega_y. \end{aligned}$$

In Eqs. (6) and (7), \mathbf{x} and \mathbf{y} represent the source and observation points, \bar{U}_{ij}, \bar{U}_i and \bar{T} are the fundamental solutions for the displacements and the temperature for homogeneous, isotropic and linear thermoelastic solids, while $\bar{T}_{ij}, \bar{T}_i, \bar{Z}_i$ and \bar{F} are the fundamental tractions and temperature gradient, respectively [Balaš; Sládek and Sládek (1989)], a tilde denotes the ratio of the non-homogeneous quantity to the corresponding homogeneous quantity that is designated by a subscript zero. The BDIEs (6) contain boundary and domain integrals with singular kernels. The strongly singular integrals are understood as the Cauchy principal value integrals. Making use of the singularity subtraction technique and the variable transformation technique, the strong and the weak singularities in Eqs. (6) can be removed [Aliabadi (2002)].

3 Numerical implementation of the BDIEM

In order to solve the BDIEs in the Laplace-transformed domain, a collocation method is employed for the spatial discretization by using quadratic elements [Aliabadi (2002)]. The boundary Γ is divided into N^q quadratic boundary elements Γ_q . After regularization the domain-integrals can be rewritten by application of the Gauss-Ostrogradsky theorem and arranging as

$$\begin{aligned} \bar{F}_j^{(u)}(\mathbf{x}, p) &= \int_{\Gamma} f_{ij}^{(1)}(\mathbf{x}, \mathbf{y}, p) \bar{u}_i(\mathbf{y}, p) d\Gamma_y + \int_{\Gamma} f_j^{(2)}(\mathbf{x}, \mathbf{y}, p) \bar{\theta}(\mathbf{y}, p) d\Gamma_y \\ &\quad + \int_{\Omega} g_{ij}^{(1)}(\mathbf{x}, \mathbf{y}, p) \bar{u}_i(\mathbf{y}, p) d\Omega_y + \int_{\Omega} g_j^{(2)}(\mathbf{x}, \mathbf{y}, p) \bar{\theta}(\mathbf{y}, p) d\Omega_y, \\ \bar{F}^{(\theta)}(\mathbf{x}, p) &= \int_{\Gamma} f_i^{(3)}(\mathbf{x}, \mathbf{y}, p) \bar{u}_i(\mathbf{y}, p) d\Gamma_y + \int_{\Gamma} f^{(4)}(\mathbf{x}, \mathbf{y}, p) \bar{\theta}(\mathbf{y}, p) d\Gamma_y \\ &\quad + \int_{\Omega} g_i^{(3)}(\mathbf{x}, \mathbf{y}, p) \bar{u}_i(\mathbf{y}, p) d\Omega_y + \int_{\Omega} g^{(4)}(\mathbf{x}, \mathbf{y}, p) \bar{\theta}(\mathbf{y}, p) d\Omega_y, \end{aligned} \tag{8}$$

where the functions $f_{ij}^{(1)}$, $f_j^{(2)}$, $f_i^{(3)}$, $f^{(4)}$ and $g_{ij}^{(1)}$, $g_j^{(2)}$, $g_i^{(3)}$ and $g^{(4)}$ are obtained from Eqs. (7), see Ekhlakov; Khay; Zhang; Sladek; Sladek and Gao (2012b) for more details. In Eqs. (8), the boundary integrals can be computed together with other boundary integrals in the BDIEs, while for computing the domain-integrals three different domain-integral evaluation techniques are tested in the present analysis. The first approach is the conventional CIM [Aliabadi (2002)], in which the interior of the domain is discretized into quadrilateral domain elements for evaluating the domain-integrals [Ekhlakov; Khay; Zhang; Sladek and Sladek (2010, 2012a)]. Although the CIM gives accurate results, the domain discretization removes the main advantages of the BEM in that only the boundary of the domain needs to be discretized into boundary elements. For this reason, two meshless techniques are considered, namely the RIM and the CTM. For convenience, the domain-integrals in Eqs. (8) can be represented without loss of generality by

$$\bar{I}^{(u)}(\mathbf{x}, p) = \int_{\Omega} \bar{G}_i(\mathbf{x}, \mathbf{y}, p) \bar{u}_i(\mathbf{y}, p) d\Omega_y, \quad \bar{I}^{(\theta)}(\mathbf{x}, p) = \int_{\Omega} \bar{G}(\mathbf{x}, \mathbf{y}, p) \bar{\theta}(\mathbf{y}, p) d\Omega_y. \tag{9}$$

In Eqs. (9), the functions \bar{G}_i and \bar{G} correspond to the functions $g_{ij}^{(1)}$, $g_i^{(3)}$ and $g_j^{(2)}$, $g^{(4)}$ from Eqs. (8), respectively. The direct transformation of the domain-integrals (9) is impracticable because they contain the unknown displacements and temperature. The unknown fields can be represented by a series of prescribed basis functions as commonly used in the DRM [Nardini and Brebbia (1983)]:

3.1 Approximation of the unknown fields

The displacements and the temperature are approximated by a series of the prescribed radial basis functions and the linear polynomials in global coordinates as

$$\bar{u}_i(\mathbf{x}, p) = \sum_{A=1}^{N_A} \alpha_i^A \varphi^A(R) + a_i^j x_j + a_i^0, \quad \bar{\theta}(\mathbf{x}, p) = \sum_{A=1}^{N_A} \beta^A \varphi^A(R) + b^j x_j + b^0, \quad (10)$$

$$\sum_{A=1}^{N_A} \alpha_i^A(p) = 0, \quad \sum_{A=1}^{N_A} \alpha_i^A(p) x_j^A = 0, \quad \sum_{A=1}^{N_A} \beta^A(p) = 0, \quad \sum_{A=1}^{N_A} \beta^A(p) x_j^A = 0, \quad (11)$$

where $\varphi^A(R)$ is the radial basis function of the distance $R = |\mathbf{x} - \mathbf{x}^A|$ from the application point A to the field point \mathbf{x} , x_j^A denotes the Cartesian coordinates of the application point A , N_A is the total number of the application points consisting of all boundary nodes and some selected internal nodes, and α_i^A , β^A , a_i^j and b^j are the unknown expansion coefficients to be determined. Here, the combination of the radial basis functions and the polynomials in terms of the global coordinates are applied to obtain satisfactory results [Chen; Golberg and Bowman (1999); Gao (2002a)]. The approximation of the unknown functions by (10) has been successfully applied for the fracture analysis of FGMs [Gao; Zhang; Sladek and Sladek (2008); Ekhlov; Khay; Zhang; Sladek; Sladek and Gao (2012b)]. The fourth order spline-type radial basis function [Gao (2002a)] is used

$$\phi^A(R) = \begin{cases} 1 - 6 \left(\frac{R}{d_A}\right)^2 + 8 \left(\frac{R}{d_A}\right)^3 - 3 \left(\frac{R}{d_A}\right)^4, & 0 \leq R \leq d_A, \\ 0, & R \geq d_A, \end{cases} \quad (12)$$

where d_A is the support size for the application point A as shown in Fig. 1a. The unknown coefficients α_i^A , β , a_i^k and b^k can be determined by applying the application point A in Eqs. (10)-(11) to every nodes. This leads to the following systems of linear algebraic equations

$$\bar{\mathbf{u}} = \mathbf{\Phi} \cdot \bar{\boldsymbol{\alpha}}, \quad \bar{\theta} = \mathbf{\Phi} \cdot \bar{\boldsymbol{\beta}}, \quad (13)$$

where $\bar{\mathbf{u}}$ and $\bar{\theta}$ denote the vectors of the displacements and the temperature at all application points A , respectively, and $\boldsymbol{\alpha}$ and $\boldsymbol{\beta}$ are the vectors consisting of the unknown coefficients α_i^A , β , a_i^k and b^k . It is assumed that the two application points do not coincide. Therefore, the square matrix $\mathbf{\Phi}$ is invertible and thereby

$$\boldsymbol{\alpha} = \mathbf{\Phi}^{-1} \cdot \bar{\mathbf{u}}, \quad \boldsymbol{\beta} = \mathbf{\Phi}^{-1} \cdot \bar{\theta}. \quad (14)$$

It should be noted that the matrix $\mathbf{\Phi}$ is uniquely determined by the location of the application points and independent of the value of the Laplace-transform parameter p . Thus, the matrix $\mathbf{\Phi}$ has to be evaluated only once.

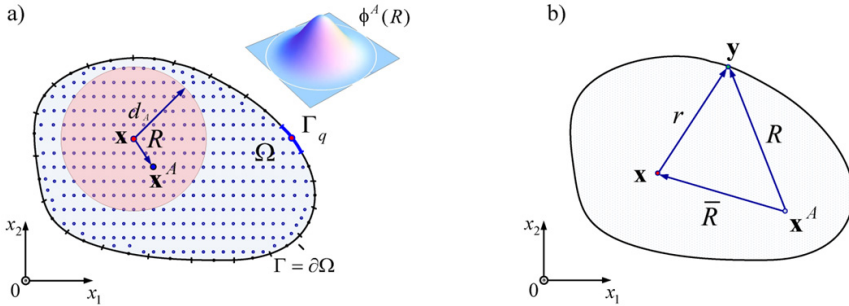


Figure 1: (a) Approximation of the unknown fields by the prescribed basis functions, (b) Relationship between distances

Substitution of Eqs. (10) into the domain-integrals of Eqs. (9) yields

$$\begin{aligned}
 \bar{I}^{(u)}(\mathbf{x}, p) &= \alpha_i^A(p) \int_{\Omega} \bar{G}_i(\mathbf{x}, \mathbf{y}, p) \varphi^A(R) d\Omega_y + a_i^k(p) \int_{\Omega} \bar{G}_i(\mathbf{x}, \mathbf{y}, p) x_k d\Omega_y \\
 &\quad + a_i^0(p) \int_{\Omega} \bar{G}_i(\mathbf{x}, \mathbf{y}, p) d\Omega_y, \\
 \bar{I}^{(\theta)}(\mathbf{x}, p) &= \beta^A(p) \int_{\Omega} \bar{G}(\mathbf{x}, \mathbf{y}, p) \varphi^A(R) d\Omega_y + b^k(p) \int_{\Omega} \bar{G}(\mathbf{x}, \mathbf{y}, p) x_k d\Omega_y \\
 &\quad + b^0(p) \int_{\Omega} \bar{G}(\mathbf{x}, \mathbf{y}, p) d\Omega_y.
 \end{aligned} \tag{15}$$

The proposed approximation of the unknown fields in Eqs. (10) is used in the RIM and the CTM.

3.2 Radial integration method

For the transformation of the appearing domain integrals $\bar{I}^{(u)}(\mathbf{x}, p)$ and $\bar{I}^{(\theta)}(\mathbf{x}, p)$ in Eqs. (9), the RIM by Gao (2002a, 2002b) can be used. Applying the RIM to the domain integrals of Eqs. (15) results in

$$\begin{aligned}
 \bar{I}^{(u)}(\mathbf{x}, p) &= \alpha_i^A(p) \int_{\Gamma} \frac{1}{r} \frac{\partial r}{\partial n} \bar{F}_i^{(1A)}(\mathbf{x}, \mathbf{y}, p) d\Gamma_y + a_i^k(p) \int_{\Gamma} \frac{r,k}{r} \frac{\partial r}{\partial n} \bar{F}_i^{(1)}(\mathbf{x}, \mathbf{y}, p) d\Gamma_y \\
 &\quad + [a_i^k(p) x_k + a_i^0(p)] \int_{\Gamma} \frac{1}{r} \frac{\partial r}{\partial n} \bar{F}_i^{(0)}(\mathbf{x}, \mathbf{y}, p) d\Gamma_y, \\
 \bar{I}^{(\theta)}(\mathbf{x}, p) &= \beta^A(p) \int_{\Gamma} \frac{1}{r} \frac{\partial r}{\partial n} \bar{F}^{(1A)}(\mathbf{x}, \mathbf{y}, p) d\Gamma_y + b^k(p) \int_{\Gamma} \frac{r,k}{r} \frac{\partial r}{\partial n} \bar{F}^{(1)}(\mathbf{x}, \mathbf{y}, p) d\Gamma_y \\
 &\quad + [b^k(p) x_k + b^0(p)] \int_{\Gamma} \frac{1}{r} \frac{\partial r}{\partial n} \bar{F}^{(0)}(\mathbf{x}, \mathbf{y}, p) d\Gamma_y.
 \end{aligned} \tag{16}$$

In Eqs. (16), the radial integrals are defined as

$$\begin{aligned}
 \bar{F}_i^{(1A)}(\mathbf{x}, \mathbf{y}, p) &= \int_0^{r(\mathbf{y})} r \bar{G}_i(\mathbf{x}, \mathbf{y}, p) \varphi^A(R) dr, & \bar{F}^{(1A)}(\mathbf{x}, \mathbf{y}, p) &= \int_0^{r(\mathbf{y})} r \bar{G}(\mathbf{x}, \mathbf{y}, p) \varphi^A(R) dr, \\
 \bar{F}_i^{(1)}(\mathbf{x}, \mathbf{y}, p) &= \int_0^{r(\mathbf{y})} r^2 \bar{G}_i(\mathbf{x}, \mathbf{y}, p) dr, & \bar{F}^{(1)}(\mathbf{x}, \mathbf{y}, p) &= \int_0^{r(\mathbf{y})} r^2 \bar{G}(\mathbf{x}, \mathbf{y}, p) dr, \\
 \bar{F}_i^{(0)}(\mathbf{x}, \mathbf{y}, p) &= \int_0^{r(\mathbf{y})} r \bar{G}_i(\mathbf{x}, \mathbf{y}, p) dr, & \bar{F}^{(0)}(\mathbf{x}, \mathbf{y}, p) &= \int_0^{r(\mathbf{y})} r \bar{G}(\mathbf{x}, \mathbf{y}, p) dr.
 \end{aligned}
 \tag{17}$$

The radial integrals in Eqs. (17) are functions of the boundary point \mathbf{y} for the boundary integrals in Eqs. (16). It is important to note here that in the integrals (16) the appearing term $r_{,k}$ is constant. The radial integrals in Eqs. (17) are regular and can be computed numerically by using standard Gaussian quadrature formula. For the evaluation of the radial integrals, the radial basis function $\varphi^A(R)$ should be expressed as a function of r . The following relations are used (see Fig. 1b)

$$y_k = x_k + r_{,k}r \quad \text{and} \quad R = \sqrt{r^2 + sr + \bar{R}^2} \quad \text{with} \quad s = 2r_{,i}\bar{R}_i.$$

3.3 Cartesian transformation method

The Cartesian transformation method by Hematiyan (2007, 2008) is another numerical method for the evaluation of the domain-integrals without domain discretization. Following the CTM, the domain-integrals $\bar{I}^{(u)}(\mathbf{x}, p)$ and $\bar{I}^{(\theta)}(\mathbf{x}, p)$ in Eqs. (15) are expressed as

$$\begin{aligned}
 \bar{I}^{(u)}(\mathbf{x}, p) &= \alpha_i^A(p) \sum_{q=1}^{N^q} \int_{\Gamma_q} \left[\int_a^{y_1(y_2)} \bar{G}_i(\mathbf{x}, \mathbf{y}, p) \varphi^A(R) dy_1^* \right] dy_2 \\
 &+ a_i^k(p) \sum_{q=1}^{N^q} \int_{\Gamma_q} \left[\int_a^{y_1(y_2)} \bar{G}_i(\mathbf{x}, \mathbf{y}, p) x_k dy_1^* \right] dy_2 \\
 &+ a_i^0(p) \sum_{q=1}^{N^q} \int_{\Gamma_q} \left[\int_a^{y_1(y_2)} \bar{G}_i(\mathbf{x}, \mathbf{y}, p) dy_1^* \right] dy_2, \\
 \bar{I}^{(\theta)}(\mathbf{x}, p) &= \beta^A(p) \sum_{q=1}^{N^q} \int_{\Gamma_q} \left[\int_a^{y_1(y_2)} \bar{G}(\mathbf{x}, \mathbf{y}, p) \varphi^A(R) dy_1^* \right] dy_2, \\
 &+ b^k(p) \sum_{q=1}^{N^q} \int_{\Gamma_q} \left[\int_a^{y_1(y_2)} \bar{G}(\mathbf{x}, \mathbf{y}, p) x_k dy_1^* \right] dy_2 \\
 &+ b^0(p) \sum_{q=1}^{N^q} \int_{\Gamma_q} \left[\int_a^{y_1(y_2)} \bar{G}(\mathbf{x}, \mathbf{y}, p) dy_1^* \right] dy_2.
 \end{aligned}
 \tag{18}$$

where a is an arbitrary constant that can be taken as the mean value of x_1 over the boundary Γ . The one-dimensional integrals in Eqs. (18) are evaluated by Gaussian quadrature formula. By using N_l integration intervals along the y_1 -direction, we obtain

$$\begin{aligned}
 \bar{I}^{(u)}(\mathbf{x}, p) &= \alpha_i^A(p) \sum_{q=1}^{N^q} J^q \sum_{i=1}^{N_i} w_i \sum_{l=1}^{N_l} J^l \sum_{j=1}^{N_j} w_j \bar{G}_i(\mathbf{x}, \mathbf{y}(\eta_i, \eta_j), p) \varphi^A(R(\eta_i, \eta_j)) \\
 &+ a_i^k(p) \sum_{q=1}^{N^q} J^q \sum_{i=1}^{N_i} w_i \sum_{l=1}^{N_l} J^l \sum_{j=1}^{N_j} w_j \bar{G}_i(\mathbf{x}, \mathbf{y}(\eta_i, \eta_j), p) x_k(\eta_i, \eta_j) \\
 &+ a_i^0(p) \sum_{q=1}^{N^q} J^q \sum_{i=1}^{N_i} w_i \sum_{l=1}^{N_l} J^l \sum_{j=1}^{N_j} w_j \bar{G}_i(\mathbf{x}, \mathbf{y}(\eta_i, \eta_j), p), \\
 \bar{I}^{(\theta)}(\mathbf{x}, p) &= \beta^A(p) \sum_{q=1}^{N^q} J^q \sum_{i=1}^{N_i} w_i \sum_{l=1}^{N_l} J^l \sum_{j=1}^{N_j} w_j \bar{G}_i(\mathbf{x}, \mathbf{y}(\eta_i, \eta_j), p) \varphi^A(R(\eta_i, \eta_j)) \\
 &+ b^k(p) \sum_{q=1}^{N^q} J^q \sum_{i=1}^{N_i} w_i \sum_{l=1}^{N_l} J^l \sum_{j=1}^{N_j} w_j \bar{G}_i(\mathbf{x}, \mathbf{y}(\eta_i, \eta_j), p) x_k(\eta_i, \eta_j) \\
 &+ b^0(p) \sum_{q=1}^{N^q} J^q \sum_{i=1}^{N_i} w_i \sum_{l=1}^{N_l} J^l \sum_{j=1}^{N_j} w_j \bar{G}_i(\mathbf{x}, \mathbf{y}(\eta_i, \eta_j), p),
 \end{aligned} \tag{19}$$

where N_i and N_j are the numbers of the integration points for the integration over the boundary element Γ_q and the l -th interval of the inner integrals, η_m , w_m and J^m are the Gaussian points, the weights and the Jacobian of the transformation, respectively. In this manner, the domain-integrals can be evaluated without domain discretization.

3.4 System of linear algebraic equations

After numerical integrations and imposing the prescribed boundary conditions the system of $3N$ linear algebraic equations can be written as

$$\begin{aligned}
 \mathbf{A}^b \mathbf{x}^b &= \mathbf{y}^b + \mathbf{D}^b \mathbf{u}, & \text{for boundary nodes,} \\
 \mathbf{A}^i \mathbf{x}^b + \mathbf{u}^i &= \mathbf{y}^i + \mathbf{D}^i \mathbf{u}, & \text{for internal nodes,}
 \end{aligned} \tag{20}$$

where $N = N^w + N^d$ is the total number of the unknown quantities, N^w and N^d correspond to the number of the boundary nodes and the number of the internal nodes, respectively, the superscripts b and i denote the quantities at a boundary point and an interior point, respectively. In Eqs. (20), \mathbf{x}^b is the $3N^w$ vector of the unknown values of the displacements \bar{u}^i , the tractions \bar{t}_i , the temperature $\bar{\theta}$ and the heat flux \bar{q} at the boundary collocation points, \mathbf{u}^i is the $3N^d$ vector of the unknown displacements \bar{u}_i and the temperature $\bar{\theta}$ at the interior collocation points, \mathbf{u} is the $3N$ vector composed of vectors \mathbf{x}^b and \mathbf{u}^i , \mathbf{y}^b and \mathbf{y}^i denote the $3N^w$ and $3N^d$ vectors of the prescribed boundary quantities. The sizes of the matrices \mathbf{A}^b , \mathbf{A}^i , \mathbf{D}^b and \mathbf{D}^i

are $3N^w \times 3N^w$, $3N^d \times 3N^w$, $3N^w \times 3N$ and $3N^d \times 3N$, respectively. It should be noted that the matrices \mathbf{D}^b and \mathbf{D}^j stem from the evaluation of the domain integrals $\bar{F}_j^{(u)}$ and $\bar{F}^{(\theta)}$. The system of linear algebraic equations (20) is solved numerically to obtain the boundary unknowns \mathbf{x}^b and the primary interior field quantities \mathbf{u}^i for discrete values of the Laplace-transform parameter p . The final time-dependent solutions are found by the numerical inversion of the Laplace transform using the Stehfest’s algorithm [Stehfest (1970)].

3.5 Computation of the stress intensity factors

There are many established methods available for the evaluation of SIFs. In this analysis, the extrapolation technique following directly from the asymptotic expansion of the displacements in the vicinity of the crack-tip is employed [Aliabadi (2002)]. The asymptotic stress and displacement fields near the crack-tip in continuously non-homogeneous and linear elastic FGMs have the same singularity and structure as those in homogeneous and linear elastic solids [Eischen (1987)]. Hence, the SIFs can also be used to linear thermoelastic FGMs. For a central crack of the length $2a$ that is located on the x_1 -axis with the crack-tips at $x_1 = \pm a$, the dynamic SIFs are related to the crack-opening-displacements $\Delta u_i(x_1, t)$ by

$$\left\{ \begin{array}{l} K_I^\pm(t) \\ K_{II}^\pm(t) \end{array} \right\} = \frac{\sqrt{2\pi}}{\kappa^\nu + 1} \mu^{\text{tip}} \lim_{x_1 \rightarrow \pm a} \frac{1}{\sqrt{a \mp x_1}} \left\{ \begin{array}{l} \Delta u_2(x_1, t) \\ \Delta u_1(x_1, t) \end{array} \right\}, \quad (21)$$

where $K_I^\pm(t)$ and $K_{II}^\pm(t)$ represent the mode-I and mode-II dynamic SIFs, $\kappa^\nu = 3 - 4\nu$ or $\kappa^\nu = (3 - \nu)/(1 + \nu)$ for plane strain or plane stress state, respectively, and μ^{tip} is the shear modulus at the crack-tips $x_1 = \pm a$. For convenience, the dynamic SIFs and the time are normalized as $\bar{K}(t) = K(t)/\alpha_0 E_0 \theta_0 \sqrt{\pi a}$ and $\bar{t} = t k_0/a^2 \rho_0 c_0$.

4 Numerical examples

To compare the three different domain-integral evaluation techniques in the presented BDIEM two thermoelastic crack problems are analyzed. In the first example, an edge crack in a rectangular, isotropic, continuously non-homogeneous and linear thermoelastic FGM plate subjected to a cooling thermal shock $\theta(\mathbf{x}, t) = -\theta_0 H(t)$ at the lateral side is considered (Fig. 2a). Here, θ_0 is the constant amplitude and $H(t)$ is the Heaviside step function. The geometry is described by the plate width $w = 1$, plate height $2h = 3w$ and crack length $a = 0.4w$. The material gradation in the x_i -direction is given by an exponential law $E(\mathbf{x}) = E_0 \exp(\alpha_g |x_i|)$, $k(\mathbf{x}) = k_0 \exp(\beta_g |x_i|)$ and $c(\mathbf{x}) = c_0 \exp(\gamma_g |x_i|)$ with the gradient parameters $\alpha_g = \ln(E_b/E_0)/\ell$, $\beta_g = \ln(k_b/k_0)/\ell$ and $\gamma_g = \ln(c_b/c_0)/\ell$, where $E_0 = E(0)$, $k_0 = k(0)$,

$c_0 = c(0)$ and $E_b = E(\ell)$, $k_b = k(\ell)$ and $c_b = c(\ell)$ are the Young's modulus, the thermal conductivity and the specific heat at the left and the right side of the plate with the material gradation in the x_1 -direction (Fig. 2b) or at the bottom and the top side of the plate with the gradation in the x_2 -direction (Fig. 2c), i.e. ℓ is equal to w or h , respectively. The mass density, the Poisson's ratio and the linear thermal expansion coefficient are taken as constant, e.g., $\rho(\mathbf{x}) = 1$, $\nu = 0.25$ and $\alpha(\mathbf{x}) = 0.02$, respectively. Plane strain condition is assumed in the numerical analysis.

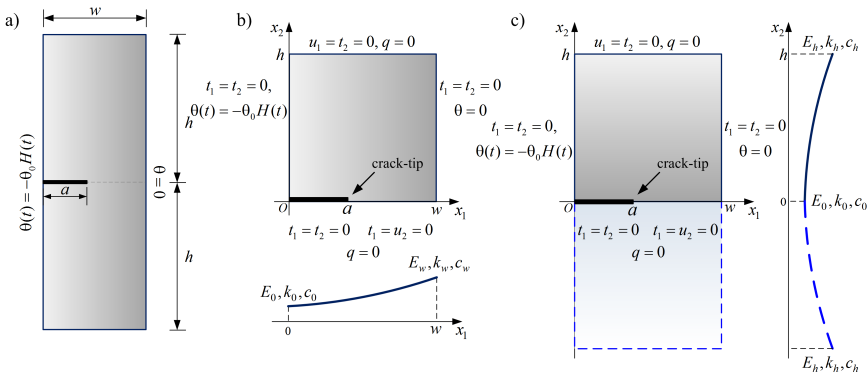


Figure 2: An edge crack in a rectangular FGM plate under thermal shock

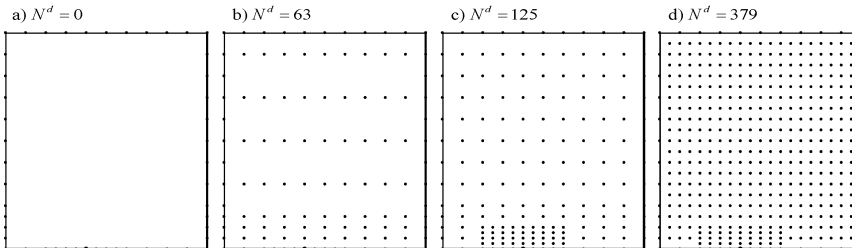


Figure 3: Different numbers of the internal nodes

Due to the selected material gradations, the symmetry of the loading conditions and the plate geometry only one half of the plate is considered in the numerical computations (Fig. 2.b-c). In this case, only the mode-I dynamic SIF occurs whereas the mode-II dynamic SIF is identically zero. The plate is discretized into 48 boundary nodes and 125 internal nodes. For a better approximation of the displacements and the temperature near the crack-tip, the density of nodes in the vicinity of the crack-tip increases towards the crack-tip.

To investigate the influence of the material gradation on the dynamic SIFs, two material gradient parameters are selected as $\alpha_g = \beta_g = \gamma_g = \pm 0.7$. In order to check the influence of the number and the distribution of internal nodes on the numerical results obtained by the meshless domain-integral evaluation techniques, the cracked plate with the material gradation in the x_1 -direction is first analyzed with 0, 63, 125 and 379 internal nodes distributed as shown in Fig. 3. Figures 4 and 5 show the normalized mode-I dynamic SIFs versus the dimensionless time obtained by the RIM and the CTM for different numbers of the internal nodes as well as by the FEM. The FEM calculations are carried out by using the multiphysics simulation code COMSOL with 8400 isoparametric quadrilateral elements. Numerical results obtained by the present BDIEM and the FEM are in a good agreement. The computed results are relatively close for different numbers of the internal nodes, which indicates that both meshless domain-integral evaluation techniques are insensitive to the used numbers of the internal nodes.

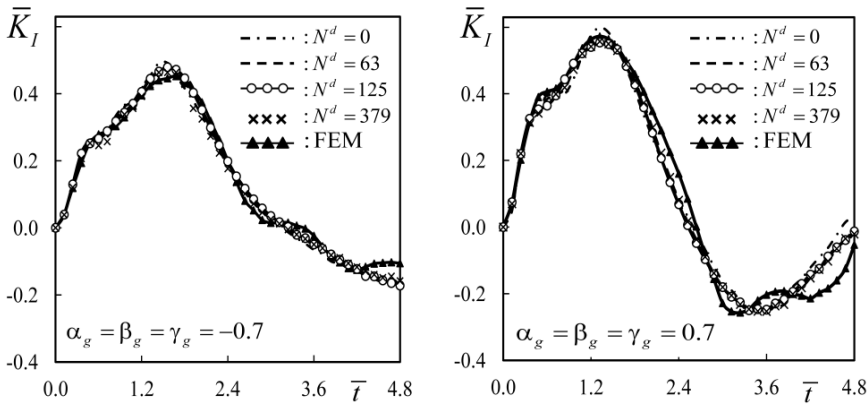


Figure 4: Effects of the number of internal nodes on SIFs obtained by RIM

To achieve a sufficient accuracy of the numerical results some internal nodes are necessary. On the other hand, a large number of the internal points will lead to a significant increase in the computational cost. The time variations of the normalized mode-I dynamic SIFs for the cracked FGM plate with the material gradations parallel (Fig. 2b) and perpendicular (Fig. 2c) to the crack-line and the gradient parameters $\alpha_g = \beta_g = \gamma_g = \pm 0.7$ are presented in Figs. 6 and 7. The numerical results obtained by all three domain-integral evaluation techniques show very a good agreement, despite some small discrepancies of the dynamic SIF obtained by the CTM in the large time range.

As second example, we consider a central crack in a rectangular FGM plate under

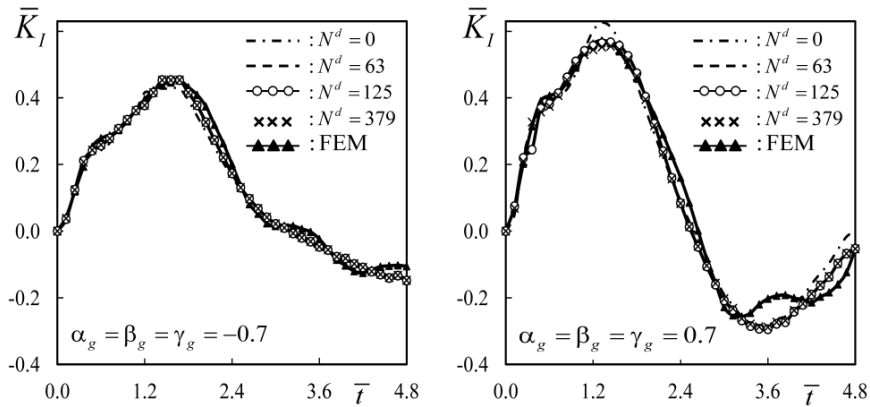


Figure 5: Effects of the number of internal nodes on SIFs obtained by CTM

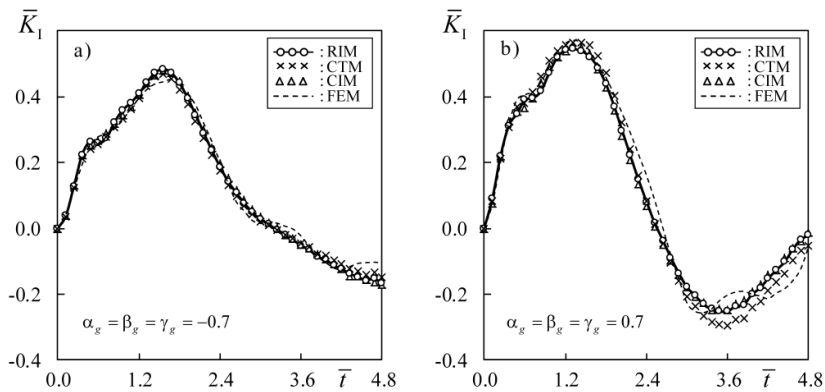


Figure 6: Comparison of the normalized mode-I dynamic SIFs obtained by the RIM, the CTM and the CIM for the material gradation in the x_1 -direction

a thermal shock (Fig. 8a). The geometry of the cracked plate is given by the width $w = 1$, height $h = 2.4w$ and crack length $2a = 0.8w$. The coordinate origin is placed at the crack center. The material gradation in the x_i -direction is assumed also to have exponential laws $E(\mathbf{x}) = E_0 \exp(\alpha_g x_i)$, $k(\mathbf{x}) = k_0 \exp(\beta_g x_i)$ and $c(\mathbf{x}) = c_0 \exp(\gamma_g x_i)$ with the same calculation parameters as in the first example.

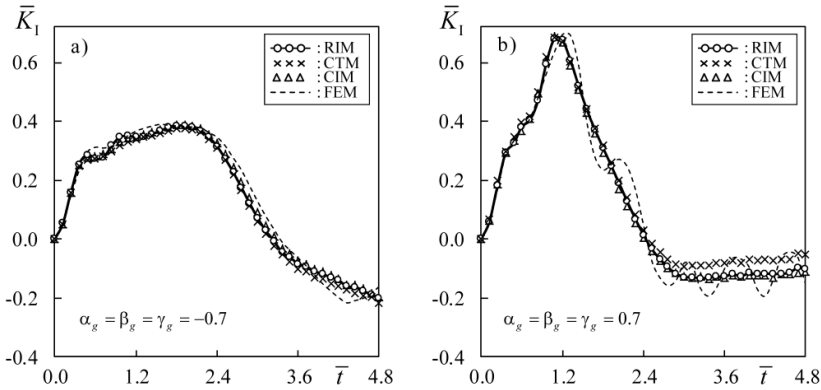


Figure 7: Comparison of the normalized mode-I dynamic SIFs obtained by the RIM, the CTM and the CIM for the material gradation in the x_2 -direction

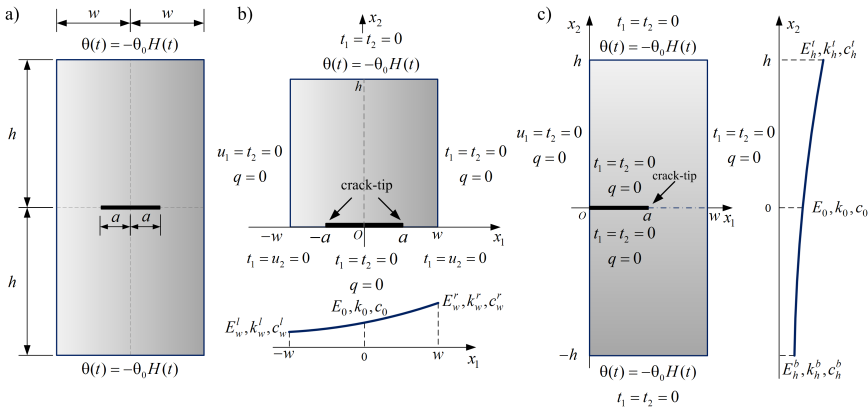


Figure 8: A central crack in a rectangular FGM plate under a thermal shock

First, the material gradation parallel to the crack-line is analyzed (Fig. 8b). By virtue of symmetry of the problem with respect to the x_1 -axis, only one half of the plate is numerically analyzed. In this case, only the mode-I dynamic SIF occurs

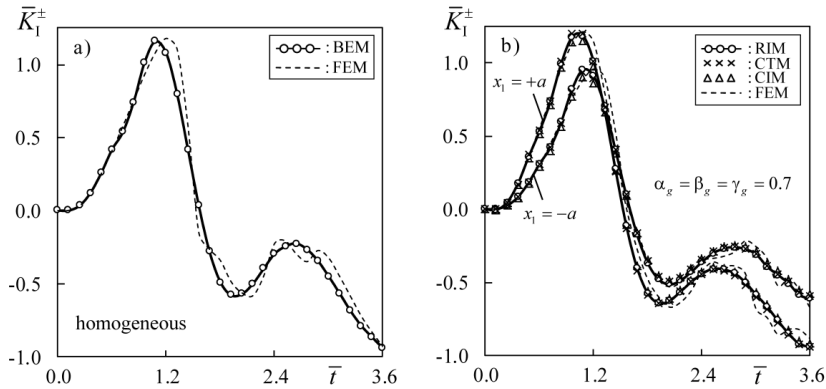


Figure 9: Normalized mode-I dynamic SIFs for the cracked homogeneous (a) and FGM (b) plate

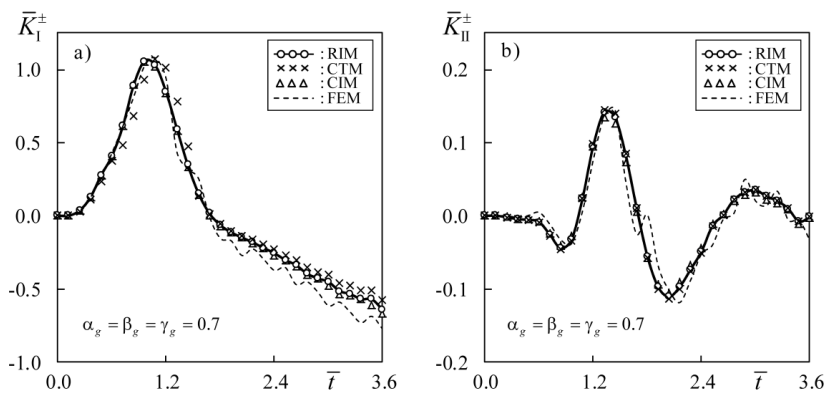


Figure 10: Comparison of the normalized dynamic SIFs obtained by the RIM, the CTM and the CIM for the material gradation in the x_2 -direction

whereas the mode-II dynamic SIF is identically zero. In this example, 48 boundary nodes and 125 internal nodes are used in the discretization. To test the accuracy of the implemented BDIEM, the normalized dynamic mode-I dynamic SIFs $\bar{K}_I^\pm(t)$ at the crack-tips $x_1 = \pm a$ for the homogeneous material ($\alpha_g = \beta_g = \gamma_g = 0$) are compared with the FEM results in Fig. 9a, which show a good agreement between both methods. The time variations of the normalized dynamic mode-I dynamic SIFs at the crack-tips $x_1 = \pm a$ obtained by the RIM, the CTM, the CIM and the FEM for the gradient parameters $\alpha_g = \beta_g = \gamma_g = 0.7$ are shown in Fig. 9b. One can observe a good agreement of the numerical results provided by the different domain-integral evaluation techniques and the FEM.

Finally, the material gradation perpendicular to the crack-line is taken for the cracked plate (Fig. 8c). Due to symmetry of the considered problem with respect to the x_2 -axis, only one half of the plate is modeled by the BDIEM as shown in Fig. 8c. The sub-domain technique is used in the present analysis [Aliabadi (2002)]. The plate is virtually divided into two sub-domains along the crack-line. The BDIEs are applied to each sub-domain and the continuity conditions on the common boundary of the sub-domains are used to obtain the final system of algebraic equations. The material non-homogeneity induces a mixed mode crack-tip loading even though the cracked plate is subjected to a pure thermal loading on the top and the bottom side symmetric to the crack-faces, i.e. the mode-II dynamic SIF is also present along with the mode-I dynamic SIF. For the discretization of the FGM plate, 64 boundary and 123 internal nodes are used. The time variations of the normalized mode-I and mode-II dynamic SIFs for the gradient parameters $\alpha_g = \beta_g = \gamma_g = 0.7$ are shown in Fig. 10. Again one can observe a good agreement among the results provided by the RIM, the CIM and the FEM, while the CTM results show some differences.

5 Conclusions

In this paper, three domain-integral evaluation techniques in the BDIEM for transient thermoelastic crack analysis in 2-D, continuously non-homogeneous, isotropic and linear thermoelastic FGMs are presented and compared. Fundamental solutions for homogeneous, isotropic and linear thermoelastic solids are used to derive the BDIEs. The material non-homogeneity is described by domain-integrals. After regularization procedures the domain-integrals are evaluated by the RIM, the CTM and the CIM. Numerical results for the dynamic SIFs are presented and discussed for a stationary crack in a finite FGM plate under a thermal shock. The following conclusions can be drawn from the present numerical analysis:

- The three implemented domain-integral evaluation techniques as presented in this paper can be used for transient thermoelastic crack analysis in FGMs.

Numerical examples for dynamic SIFs show that the domain-integral evaluation techniques are quite accurate and robust.

- The two meshless methods for computing the domain-integrals are quite insensitive with respect to the used number of the internal nodes. To achieve a sufficient accuracy of the numerical results, much fewer internal nodes are required than in the CIM. The two meshless methods based on RIM and CTM can be easily implemented.
- The order of singularity of the integrands can be reduced by one in the RIM. Consequently, the weakly singular integrals can be computed directly.
- Regarding the computational efficiency, the two implemented meshless methods are fast while the CIM requires more internal points to obtain satisfactory results. The CTM is the fastest method. However, the RIM gives the most accurate results than other methods. Their computational cost can be significantly reduced when the radial integrals (17) can be evaluated analytically.

Acknowledgement

This work is supported by the German Research Foundation (DFG, Project-No.: ZH 15/10-2), which is gratefully acknowledged.

References

- Aliabadi, M. H.** (2002): *The Boundary Element Method: Applications in Solids and Structures*. John Wiley & Sons.
- Anlas, G.; Santare, M. H.; Lambros, J.** (2000): Numerical calculation of stress intensity factors in functionally graded materials. *Int. J. Fracture*, vol. 104, no 2, pp. 131-143.
- Balaš, J.; Sládek, J.; Sládek, V.** (1989): *Stress Analysis by Boundary Element Methods*. Elsevier.
- Cannarozzi, A.A.; Ubertini, F.** (2001): A mixed variational method for linear coupled thermoelastic analysis. *Int. J. Solids Struct.*, vol. 38, pp. 717-739.
- Chen, C. S.; Golberg, M. A.; Bowman, H.** (1999): Some recent results and proposals for the use of radial basis functions in the BEM. *Eng. Anal. Boundary Elem.*, vol. 23, no. 4, pp. 285-296.
- Dong, L.; Atluri, S. N.** (2012): SGBEM (Using Non-hyper-singular Traction BIE), and Super Elements, for Non-Collinear Fatigue-growth Analyses of Cracks

in Stiffened Panels with Composite-Patch Repairs. *CMES: Comput. Model. Eng. Sci.*, vol. 89, no. 5, pp. 417-458.

Dong, L.; Atluri, S. N. (2013a). Fracture & Fatigue Analyses: SGBEM-FEM or XFEM? Part 1: 2D Structures. *CMES: Comput. Model. Eng. Sci.*, vol. 90, no. 2, pp. 91-146.

Dong, L.; Atluri, S. N. (2013b). Fracture & Fatigue Analyses: SGBEM-FEM or XFEM? Part 2: 3D solids. . *CMES: Comput. Model. Eng. Sci.*, vol. 90, no. 5, pp. 379-413.

Eischen, J. W. (1987): Fracture of nonhomogeneous materials. *Int. J. Fract.*, vol. 34, no. 1, pp. 3-22.

Ekhlakov, A. V.; Khay, O. M.; Zhang, C.; Sladek, J.; Sladek, V. (2010): Transient coupled thermoelastic crack analysis in functionally graded materials. *SDHM: Structural Durability & Health Monitoring*, vol. 6, no. 4, pp. 329-350.

Ekhlakov, A. V.; Khay, O. M.; Zhang, C.; Sladek, J.; Sladek, V. (2012a): A BDEM for transient thermoelastic crack problems in functionally graded materials under thermal shock. *Comput. Mater. Sci.*, vol. 57, pp.30-37.

Ekhlakov, A. V.; Khay, O. M.; Zhang, C.; Sladek, J., Sladek, V. and Gao, X. W. (2012b): Thermoelastic crack analysis in functionally graded materials and structures by a BEM. *Fatigue Fract. Engng. Mater. Struct.*, vol. 35, pp.742-766.

Gao, X. W. (2002a): A boundary element method without internal cells for two-dimensional and three-dimensional elastoplastic problems. *J. Appl. Mech.*, vol. 69, no. 2, pp. 154-160.

Gao, X. W. (2002b): The radial integration method for evaluation of domain integrals with boundary-only discretization. *Eng. Anal. Boundary Elem.*, vol. 26, pp. 905-916.

Gao, X. W.; Zhang, C.; Sladek, J.; Sladek, V. (2008): Fracture analysis of functionally graded materials by a BEM. *Compos. Sci. Technol.*, vol. 68, pp. 1209-1215.

Greengard, L.; Rokhlin, V. (1987): A fast algorithm for particle simulations. *J. Comput. Phys.*, vol. 73, no. 2, pp. 325-348.

Hematiyan, M. R. (2007): A general method for evaluation of 2D and 3D domain integrals without domain discretization and its application in BEM. *Comput. Mech.*, vol. 39, no. 4, pp. 509-520.

Hematiyan, M. R. (2008): Exact transformation of a wide variety of domain integrals into boundary integrals in boundary element method. *Commun. Numer. Methods Eng.*, vol. 24, no. 11, pp. 1497-1521.

Hosseini-Tehrani, P.; Hosseini-Godarzi, A. R.; Tavangar, M. (2005): Boundary

element analysis of stress intensity factor K_I in some two-dimensional dynamic thermoelastic problems. *Eng. Anal. Boundary Elem.*, vol. 29, no. 3, pp. 232-240.

Keramidas, G.A.; Ting, E.C. (1976): A finite element formulation for thermal stress analysis. I. Variational formulation, II. Finite element formulation. *Nucl. Eng. Des.*, vol. 39, pp. 267-287.

Nardini, D.; Brebbia, C. A. (1983): A new approach to free-vibration analysis using boundary elements. *Applied Mathematical Modelling*, vol. 7, no. 3, pp. 157-162.

Nowak, A. J.; Brebbia, C. A. (1989): The multiple-reciprocity method - a new approach for transforming BEM domain integrals to the boundary. *Eng. Anal. Boundary Elem.*, vol. 6, no. 3, pp. 164-167.

Sladek, J.; Sladek, V.; Zhang, C. H. (2005): An advanced numerical method for computing elastodynamic fracture parameters in functionally graded materials. *Comput. Mater. Sci.*, vol. 32, no. 3-4, pp. 532-543.

Sladek, J.; Sladek, V.; Zhang, C. H.; Tan, C. L. (2006): Meshless Local Petrov-Galerkin Method for linear coupled thermoelastic analysis. *CMES: Comput. Model. Eng. Sci.*, vol. 16, no. 1, pp. 57-68.

Sladek, J.; Sladek, V.; Solek, P.; Atluri, S.N. (2008a): Modeling of intelligent material systems by the MLPG. *CMES: Comput. Model. Eng. Sci.*, vol. 34, no. 3, pp. 273-300.

Sladek, J.; Sladek, V.; Tan, C.L.; Atluri, S.N. (2008b): Analysis of transient heat conduction in 3D anisotropic functionally graded solids by the MLPG. *CMES: Comput. Model. Eng. Sci.*, vol. 32, no. 3, pp. 161-174.

Sladek, J.; Sladek, V.; Solek, P.; Tan, C.L.; Zhang, C. H. (2009): Two- and three-dimensional transient thermoelastic analysis by the MLPG-Method. *CMES: Comput. Model. Eng. Sci.*, vol. 47, no. 1, pp. 61-95.

Stehfest, H. (1970): Numerical inversion of Laplace transforms. *Commun. ACM*, vol. 13, no. 1, pp. 47-49.

Suresh, S.; Mortensen, A. (1998): *Fundamentals of Functionally Graded Materials: Processing and Thermomechanical Behaviour of Graded Metals and Metal-Ceramic Composites*. IOM Commun.